Nanostructured Li2S–C Composites as Cathode Material for High-Energy Lithium/Sulfur Batteries

ARTICLE *in* NANO LETTERS · NOVEMBER 2012

Impact Factor: 13.59 · DOI: 10.1021/nl303965a · Source: PubMed

4 AUTHORS, INCLUDING:

Kunpeng Cai
Sysmex
7 PUBLICATIONS **103** CITATIONS
SEE PROFILE

Elton J Cairns
University of California, Berkeley
236 PUBLICATIONS **7,359** CITATIONS
SEE PROFILE

NANO LETTERS

Letter

pubs.acs.org/NanoLett

Nanostructured Li_2S–C Composites as Cathode Material for High-Energy Lithium/Sulfur Batteries

Kunpeng Cai,[†,∥,⊥] Min-Kyu Song,[†,∥] Elton J. Cairns,[‡,§] and Yuegang Zhang*[,†,#]

[†]The Molecular Foundry, Lawrence Berkeley National Laboratory, Berkeley, California 94720, United States

[‡]Environmental Energy Technologies Division, Lawrence Berkeley National Laboratory, Berkeley, California 94720, United States

[§]Department of Chemical and Biomolecular Engineering, University of California, Berkeley, California 94720, United States

Supporting Information

ABSTRACT: With a theoretical capacity of 1166 mA·h·g^{-1}, lithium sulfide (Li_2S) has received much attention as a promising cathode material for high specific energy lithium/sulfur cells. However, the insulating nature of Li_2S prevents the achievement of high utilization (or high capacity) and good rate capability. Various efforts have been made to ameliorate this problem by improving the contact between Li_2S and electronic conductors. In the literature, however, a relatively high capacity was only obtained with the Li_2S content below 50 wt %; therefore, the estimated cell specific energy values are often below 350 W·h·kg^{-1}, which is insufficient to meet the ever-increasing requirements of newly emerging technologies. Here, we report a cost-effective way of preparing nanostructured Li_2S-carbon composite cathodes by high-energy dry ball milling of commercially available micrometer-sized Li_2S powder together with carbon additives. A simple but effective electrochemical activation process was used to dramatically improve the utilization and reversibility of the Li_2S–C electrodes, which was confirmed by cyclic voltammetry and electrochemical impedance spectroscopy. We further improved the cycling stability of the Li_2S–C electrodes by adding multiwalled carbon nanotubes to the nanocomposites. With a very high specific capacity of 1144 mA·h·g^{-1} (98% of the theoretical value) obtained at a high Li_2S content (67.5 wt %), the estimated specific energy of our cell was ~610 W·h·kg^{-1}, which is the highest demonstrated so far for the Li/Li_2S cells. The cells also maintained good rate capability and improved cycle life. With further improvement in capacity retention, nanostructured Li_2S–C composite cathodes may offer a significant opportunity for the development of rechargeable cells with a much higher specific energy.

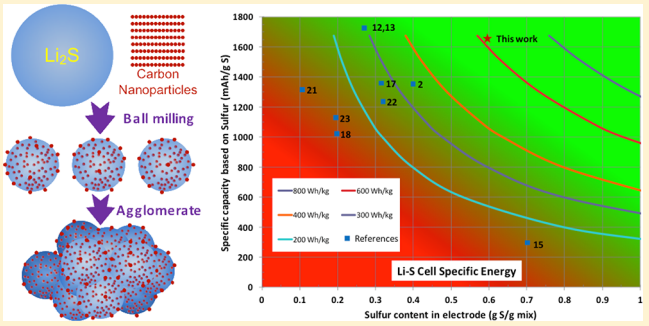

KEYWORDS: *Energy storage, lithium/sulfur batteries, lithium sulfide (Li_2S), cathodes, high specific energy, electrochemical activation*

Newly emerging technologies such as electric vehicles (EV) and advanced portable electronics are placing a strong and urgent demand on the next generation of rechargeable batteries with high specific energy.[1−7] Current lithium-ion cells with oxide-based cathodes, such as $LiCoO_2$ and $LiMn_2O_4$, have theoretical specific energies of approximately 430−570 W·h·kg^{-1}, but their practical (or obtainable) specific energies are only in the range of 120−200 W·h·kg^{-1}, which is insufficient for long EV driving ranges (i.e., >300 km).[8−11] In this regard, the lithium/sulfur cell is considered to be a potential candidate to replace current lithium-ion cells because its theoretical specific energy and volumetric energy density are estimated to be 2600 W·h·kg^{-1} and 2800 W·h·L^{-1}, respectively, based on the electrochemical reaction $16Li + S_8 = 8Li_2S$.[12−14] Additionally, the abundant availability and low price of sulfur offer the opportunity for a significant cost reduction.

However, the insulating nature of sulfur, dissolution and shuttling of lithium polysulfides during cycling, and their high reactivity with the lithium metal anode, together with significant volume change, are currently preventing the use of this promising system in practical applications.[2,15,16] Recently, the lithium sulfide (Li_2S) cathode, with a theoretical capacity of 1166 mA·h·g^{-1}, has received much attention due to the potential to use non-lithium anodes; other high-capacity anode materials (e.g., silicon or tin-based compounds which can form alloys with lithium) can be used as negative electrodes with improved safety. To resolve the insulating problem of Li_2S that prevents the achievement of high utilization (or high capacity), various efforts have been made to improve the contact between Li_2S and electronic conductive additives such as carbon and metals. Cui's group reported a lithium-free cell consisting of a Li_2S-mesoporous carbon composite as a cathode and silicon nanowires as an anode. Li_2S was better utilized by incorporating it within the small pores of CMK-3 mesoporous carbon.[2] Improved performance of electrodes made from ball-milled Li_2S powders (~10 μm) and super-P carbon was reported by Scrosati's group.[12,13] Recently, a high charging cutoff voltage

Received: October 27, 2012
Revised: November 23, 2012

   dx.doi.org/10.1021/nl303965a | *Nano Lett.* XXXX, XXX, XXX−XXX

was reported by Cui's group to activate ball-milled, micrometer-sized Li_2S (1−10 μm) particles and improve the kinetics of Li_2S.[17] The application of Li_2S-based electrodes in all-solid state cells was also studied by Tatsumisago et al., who prepared Li_2S−Cu and Li_2S−Cu−C composites as cathodes.[18,19] Other Li_2S-metal (Co, Fe) composites were also investigated as potential cathodes with some improvement.[20] A spark-plasma induced sintering process was introduced to prepare Li_2S-carbon composite electrodes with strong binding between Li_2S and carbon, which exhibited a good discharge capacity of 920 mA·h·g^{-1} of Li_2S.[21]

Despite these efforts, a relatively high capacity could only be obtained when the Li_2S content is lower than 50 wt %, while higher Li_2S contents often resulted in very low discharge capacity (i.e., only ∼200 mA·h·g^{-1} at 76.8 wt %).[2,12,13,15,18,19,21−23] To meet the rigorous requirements of high specific energy for EV applications, we need to dramatically increase the loading of Li_2S while maintaining good electrochemical utilization and good cycle life. Here, we report a simple, cost-effective high-energy dry ball milling method for preparing nanostructured Li_2S-carbon composites using commercially available micrometer-sized Li_2S powder. A simple one-step electrochemical activation process was used to dramatically improve the utilization and reversibility of Li_2S electrodes. Even with much higher Li_2S contents (67.5 wt %), the Li_2S-carbon nanocomposite cathodes exhibited a first-cycle discharge capacity of 1144 mA·h·g^{-1} based on Li_2S (98% of the theoretical value), while maintaining good rate capability and improved cycle life. This gives an estimated cell specific energy of ∼610 W·h·kg^{-1} (including all components except cell housing) for Li/Li_2S cells, the highest value demonstrated so far for such systems.

The typical morphology of commercial Li_2S powder is shown in Figure 1a. The particle size is between 10 and 30 μm, which poses difficulties in efficiently converting lithium sulfide to sulfur ($8Li_2S \rightarrow 16Li + S_8$) due to the insulating nature of Li_2S.

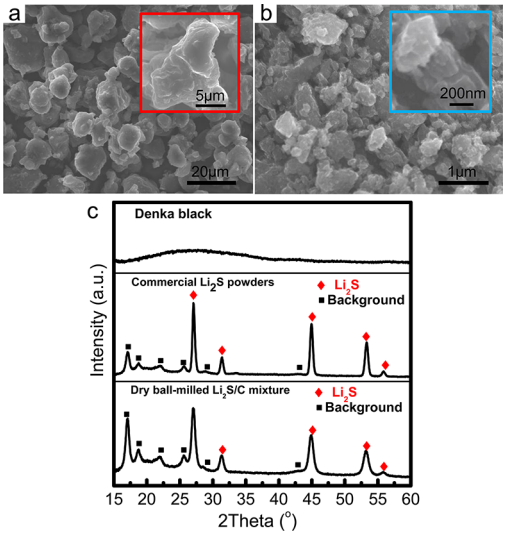

Figure 1. SEM images of (a) commercial Li_2S powder, (b) ball milled Li_2S−C composite. The insets in a and b show enlarged views of Li_2S particles before and after high-energy dry ball milling. (c) X-ray diffraction patterns of carbon black, commercial Li_2S powder and ball-milled Li_2S−C nanocomposite. The black squares indicate peaks from the glass substrate and tape cover used to prevent the exposure of Li_2S to air.

To reduce the particle size of the Li_2S and improve the current collecting capability of the cathodes, high-energy dry ball milling was applied to the Li_2S powder, which was premixed with carbon black (Denka Black) at a certain ratio (see the experimental part for details). A schematic of the electrode fabrication process is shown in Figure S1. After high-energy dry ball milling for 2 h, the size of Li_2S particles was reduced to about 200−500 nm with some agglomeration, while carbon black was found to be uniformly dispersed and deposited onto the surface of these smaller Li_2S particles. The short diffusion length associated with much smaller dimensions of nanostructured Li_2S−C electrodes can effectively reduce the distance that Li-ions and electrons must travel during cycling in the solid state. It is noted that the agglomerates are not individual Li_2S particles but rather consist of nanostructured Li_2S−C composites and the porous structure of the Li_2S−C was maintained inside the agglomerates (see Figure S2 in the Supporting Information). This structure can increase the contact area between Li_2S electrode and electrolyte, and hence the number of active sites for electrochemical reaction, which in turn reduces electrode polarization loss and improves the utilization of the active electrode material, Li_2S. Under dry ball-milling conditions, the carbon particles become strongly bonded to the Li_2S particles, which agglomerate, as shown in Figure S1c. Moreover, the small Li_2S particles are uniformly mixed with carbon black powder, which can provide the Li_2S−C composite cathode with improved current collection capability, thus a better rate capability.

X-ray diffraction (XRD) analysis was carried out to understand the composition and structural change of Li_2S powders before and after high-energy dry ball milling. A representative broad peak of carbon black was observed in Figure 1c, and the Li_2S phase was confirmed in the commercial powders. XRD peaks of the ball-milled Li_2S−C composite were found at the same position for each component, which indicates that no chemical reaction had taken place during the high-energy ball milling process. Furthermore, broadening of the peaks is observed for Li_2S, confirming that the average particle size of the Li_2S powder is reduced during the high-energy dry ball milling. The average crystallite size of Li_2S from the full width at half-maximum is estimated as ∼311 nm, which agrees well with our SEM observation. The reduced particle size of Li_2S and improved bonding between Li_2S and carbon black induced by high-energy dry ball milling offers promise for the Li_2S−C nanocomposite as a cathode material for lithium/sulfur cells.

To evaluate the electrochemical performance of the Li_2S−C nanocomposite, we fabricated cells using lithium metal anodes and cathodes made from the Li_2S−C composite and styrene-butadiene rubber (SBR) binder. The total Li_2S content was 67.5 wt %, which is much higher than that for other reports. As the Li_2S−C composite electrode is assembled in the discharged (reduced) state of sulfur, an effective activation process is essential to convert Li_2S into lithium and sulfur, whereby a sequence of intermediate polysulfides, Li_2S_x ($2 \leq x \leq 8$), are produced during the charging process. Figure 2a shows a typical cyclic voltammogram of the Li_2S−C cathode for 10 cycles. An oxidation peak is observed during charging between 2.5 and 2.8 V in the first cycle, which indicates the decomposition of Li_2S into sulfur and/or polysulfides. In the subsequent cathodic scan, three reduction peaks are observed, which correspond to the stepwise electrochemical reduction of elemental sulfur to Li_2S. Two oxidation peaks are developed in the second anodic

dx.doi.org/10.1021/nl303965a | Nano Lett. XXXX, XXX, XXX−XXX

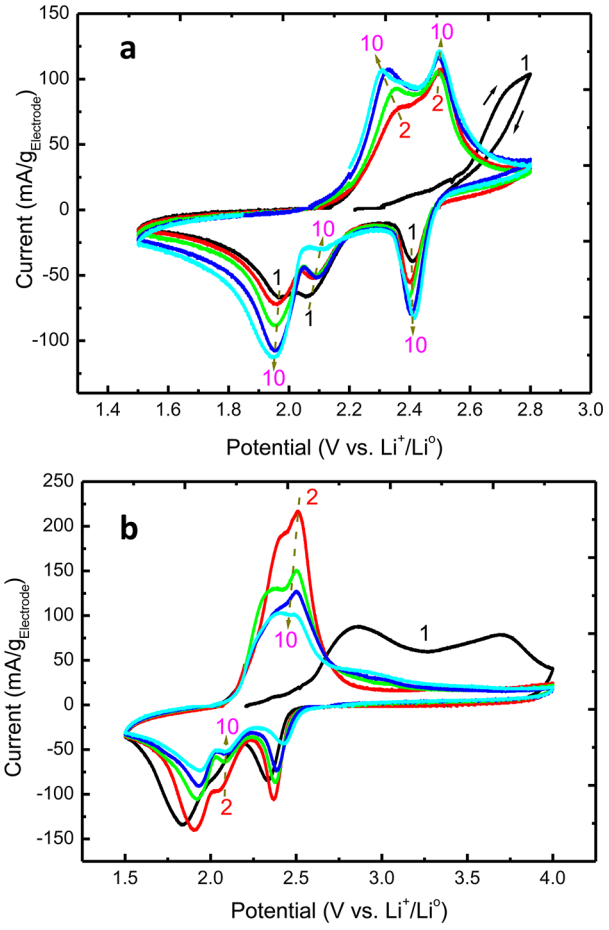

Figure 2. Cyclic voltammograms of Li_2S–C nanocomposite cathodes with different cutoff potentials: (a) 1.5–2.8 V and (b) 1.5–4.0 V, where 1, 2, 4, 6, and 10 cycles are shown. The scan rate was 0.04 $mV \cdot s^{-1}$.

scan (charging), while the three reduction peaks are maintained in the second cathodic scan (discharging). The height of these peaks (except for the small reduction peak near 2.1 V) is found to increase for two subsequent cycles, indicating increased charge and discharge capacity. After the initial 6 cycles, the heights of the main peaks were found to remain at a similar level in subsequent cycles (6–10), indicating good reversibility. It should be mentioned that, however, although the oxidation peak is clearly observed in the first charging, the corresponding current is still significantly positive at 2.8 V, which raises a question as to whether 2.8 V is enough to achieve the full conversion of Li_2S into S or not.

To further investigate this issue, we applied another potential range between 1.5 and 4.0 V. The first anodic scan in Figure 2b shows two broad oxidation peaks (at 2.8 and 3.7 V), the integral of which is far greater than that obtained in Figure 2a, indicating higher charge capacity obtained in this high cutoff potential activation process. In the following cathodic scan, discharging peaks were observed at similar positions to those shown in Figure 2a, but with much higher discharge capacity. Thus, both the initial charge and the discharge capacities were effectively improved when the cutoff charging potential is increased from 2.8 to 4.0 V in the first cycle. At the second charge, only one oxidation peak (with a shoulder at a slightly lower potential) appeared with a much greater peak height, implying that the first charge up to 4 V effectively converted Li_2S to S. Also, the peak heights decline quickly in the subsequent cycles between 1.5 and 4.0 V. In comparing Figure 2a and b, it is noted that this fast decay might result from side reactions; currents are still positive in the high potential range (2.8–4.0 V). Noting this, we developed a testing protocol in which a cutoff potential of 4.0 V was used only for the first activation cycle for the as-prepared Li_2S–C composite cell, while a 1.5–2.8 V range was used in all subsequent cycles.

This electrochemical activation behavior was also confirmed by the electrochemical impedance spectra collected at different stages of charging up to 4.0 V with a constant current of 33.5 $mA \cdot g^{-1}$ based on Li_2S. As shown in Figure 3, the diameter of

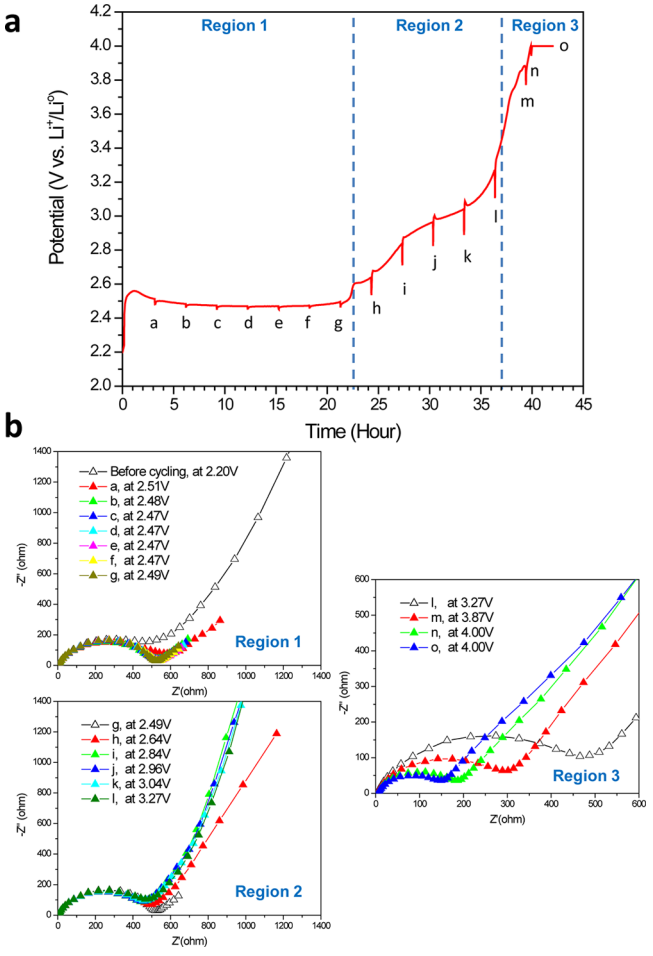

Figure 3. Electrochemical impedance spectra collected during constant current charging up to 4 V. (a) First charge profile with a constant current of 33.5 $mA \cdot g^{-1}$ of Li_2S. (b) Impedance spectra collected at every 3 h. The diameter of semicircle decreases dramatically above 3.7 V, indicating that the charge transfer resistance of Li_2S electrodes was significantly reduced. Below 3.7 V, however, only the long linear tail changed, indicating that a microstructural change of the Li_2S electrode occurred.

the semicircle (corresponding to the charge transfer resistance at the interface) started to decrease dramatically after the cell was charged above 3.7 V, implying that sulfur cathode becomes noticeably more active. However, below 3.7 V, only the long linear tail at low frequency (corresponding to the mass transfer resistance) changed, which indicates that the microstructure of the electrode changed significantly during regions 1 and 2. From the changes in the impedance spectra and cyclic

dx.doi.org/10.1021/nl303965a | *Nano Lett.* XXXX, XXX, XXX–XXX

voltamograms, we have concluded that the initial charging of the Li_2S cell up to 4 V is critical to improving the S utilization and reducing the charge transfer resistance of Li_2S electrodes. The high charging cutoff voltage was believed to be very critical for overcoming the initial potential barrier for phase nucleation of polysulfides as discussed in the recent work from Cui's group.[17] This initial potential barrier can also be seen in Figure 3a, partly confirming the proposed mechanism in Cui's work. In our case, we observed a much more reduced height of the potential barrier, which can be attributed to the smaller Li_2S particle size (compared to 1−10 μm of ball-milled Li_2S in Cui's work) and strong bonding between Li_2S and carbon in our cathode material formed during high-energy dry ball milling of Li_2S powder together with carbon.

The electrode fabrication conditions significantly influenced the morphology of as-prepared Li_2S−C electrodes, the size of Li_2S particles, and their electrochemical performance. A summary of the cathode composition and various ball-milling conditions is given in Table S1. It is worth pointing out that the formation of Li_2S−C agglomerates during the high-energy dry milling process helped build strong bonds between the Li_2S and the carbon black, which can improve the current collecting capability and mitigate the shuttling of polysulfides, hence showing much better utilization and capacity retention, when compared to wet-milled Li_2S−C mixtures. As demonstrated in Figure S3, it took longer cycles to activate a cathode made from wet-milled powders than that from dry-milled powders. The poor performance of electrodes made from wet-milled Li_2S could be attributed to the large particle size of the Li_2S and poor bonding between Li_2S and carbon black as shown in Figure S4, indicating that carbon and Li_2S must be in intimate contact to make effective utilization of Li_2S electrode. All samples in this work were prepared using dry milling unless indicated otherwise.

Figure 4a shows the first charge/discharge profiles for the Li_2S−C nanocomposite cathode. The discharge curve exhibits three clear plateaus around 2.4, 2.1, and 2.0 V, illustrating the conversion of sulfur to high-order polysulfides, high-order polysulfides to lower-order polysulfides, and lower-order polysulfides to solid Li_2S (and possibly Li_2S_2), respectively. The first discharge of the Li_2S−C composite cathode exhibited a very high specific capacity of 1144 mA·h·g^{-1} with respect to Li_2S, which approaches the theoretical capacity (1166 mA·h·g^{-1}) of Li_2S, implying that almost all of the Li_2S was converted to S in the activation procedure (the first charge) and that the S was effectively converted back to Li_2S during the first discharge at a C/50 rate. Charge and discharge profiles of the subsequent cycles are similar to those reported for typical Li/S cells, as shown in Figure 4b, where the voltage profiles obtained at the C/10 rate are shown.

The cycling performance of the Li_2S−C composite cathode is shown in Figure 4c, with an initial discharge capacity of 1144 mA·h·g^{-1} based on Li_2S (or 1642 mA·h·g^{-1} based on S). Although capacity fading is observed during cycling, the nanostructured Li_2S−C composite cathode still exhibits a good capacity of 411 mA·h·g^{-1} based on Li_2S (or 590 mA·h·g^{-1} based on S) at the C/10 rate after 50 cycles. This capacity fading could be attributed to the "shuttle" phenomenon of lithium polysulfides, which leads to the loss of active material and reduction in both charge and discharge capacities.[24] Another possibility is mechanical degradation of the electrode structure due to repeated expansion and contraction that accompanies the conversion of S to Li_2S and back again. The

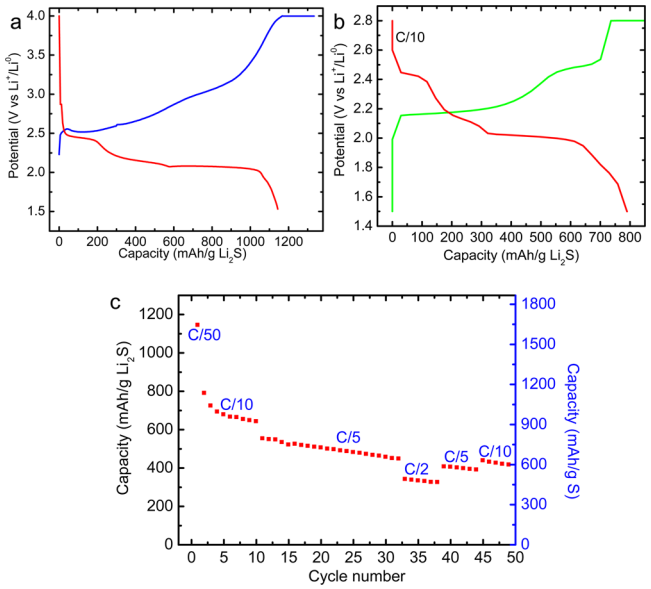

Figure 4. (a) Voltage profiles with the first activation cycle at a rate of C/50 up to 4 V. The Coulombic efficiency was estimated as ∼98.1%. The constant-current constant-voltage (CCCV) charging method was used in all cycles. (b) Voltage profiles at a discharging rate of C/10. The Coulombic efficiency was estimated as ∼96.6%. The voltage range was changed to 1.5−2.8 V in subsequent cycles. (c) Cycling performance of Li_2S−C composite electrodes. The capacity is normalized both by the weight of Li_2S and sulfur. The average loading of the electrodes is 0.794 mg·cm^{-2}, which corresponds to 0.54 mg·cm^{-2} of Li_2S.

cells also showed good rate capability by exhibiting a discharge capacity of 552 mA·h·g^{-1} based on Li_2S (or 792 mA·h·g^{-1} based on S) and 342 mA·h·g^{-1} based on Li_2S (or 491 mA·h·g^{-1} based on S) at 0.2C and 0.5C, respectively. Voltage profiles of this Li_2S−C composite electrode obtained at different C-rates are shown in Figure S5.

To further improve the conductivity and capacity retention of the Li_2S−C composite cathode, we have added multiwalled carbon nanotubes (MWCNTs) to the electrode. The long and thin MWCNTs can form three-dimensionally porous, electronically conducting network structures, which can lead to improved electrochemical performance of Li_2S electrodes. As shown in Figure 5a, indeed, the addition of MWCNTs creates more porous structures on the surface of the Li_2S−C agglomerate, which can facilitate electron transport while allowing fast lithium ion transport. As shown in Figure 5b, the addition of 5 wt % of MWCNTs showed improvement in cycling performance. After 50 cycles at different C-rates (0.02C, 0.1C, and 0.2C), the Li_2S−C-MWCNT composite cathode still exhibited a good discharge capacity of 455 mA·h·g^{-1} based on Li_2S (or 653 mA·h·g^{-1} based on S) at 0.2C (vs 411 mA·h·g^{-1} at 0.1C for electrodes without the addition of MWCNTs). The role of carbon nanofibers as a conductive framework was previously investigated by our group.[25,26] Due to the strong adsorption property, the micropores of the MWCNTs may also retard the diffusion of dissolved polysulfides, thus reducing the loss of the active material.[27] Furthermore, this porous electrode structure can help in accommodating the volume change (∼76%) during cycling. The cycling performance of nanostructured Li_2S−C electrode is expected to be improved further with either polysulfide or $LiNO_3$ additive in the electrolyte, as reported by Cui's group.[17] $LiNO_3$ can prevent the polysulfide

dx.doi.org/10.1021/nl303965a | Nano Lett. XXXX, XXX, XXX−XXX

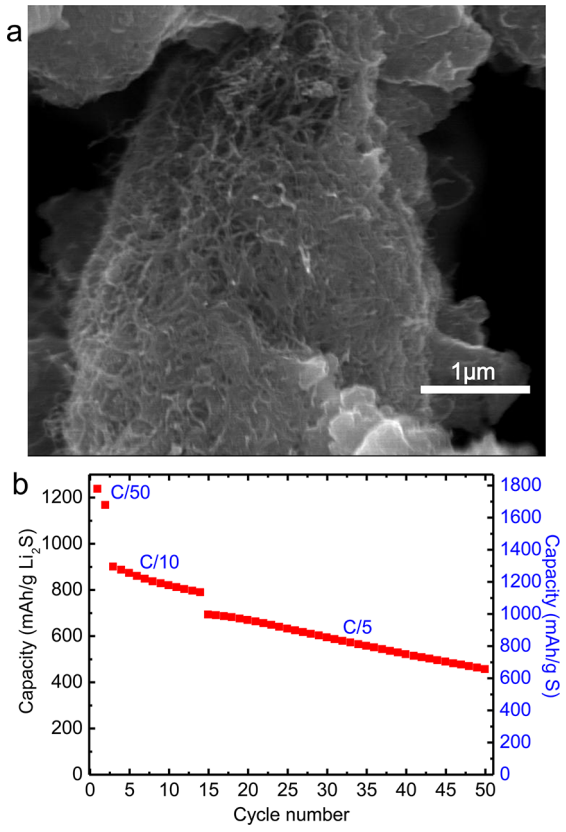

Figure 5. (a) SEM image of high-energy dry ball-milled Li_2S–C-MWCNT nanocomposite. (b) Cycling performance of Li_2S–C-MWCNTs composite cathodes at different C-rates.

shuttle by effectively passivating the lithium metal surface, which can prevent the chemical reaction of polysulfide species in the electrolyte with the lithium electrode.

With the very high specific capacity of 1144 mA·h·g^{-1} obtained at high Li_2S content (67.5 wt %), the estimated specific energy of a cell was ~610 W·h·kg^{-1}, which is the highest specific energy reported for Li/Li_2S cells. The specific energy values estimated from recent publications are shown in the Li_2S cell specific energy plot (Figure 6) for comparison purposes, where the first discharge capacity and content (%) of Li_2S in the cathode are reported based on the S content. Details of the calculation are given in Table S2. It was clearly shown that, in the literature, high specific capacity is obtained when the S is below 40% (or the Li_2S content is below 50 wt %); therefore, the estimated cell specific energy values are often below 350 W·h·kg^{-1}, which is insufficient to meet the ever-increasing requirements of emerging energy storage applications such as electric vehicles.

To summarize, we have developed a cost-effective high-energy dry ball milling method to prepare nanostructured Li_2S–C composite cathodes using commercial micrometer-sized Li_2S powders. We also demonstrated a simple, but very effective electrochemical activation process allowing nearly full conversion of Li_2S to sulfur, which was confirmed by cyclic voltammetry and electrochemical impedance spectroscopy. Thus, Li_2S–C nanocomposite cathodes of high Li_2S content exhibited a discharge capacity of 1144 mA·h·g^{-1} based on Li_2S (98% of theoretical value; 1643 mA·h·g^{-1} based on S) with good rate capability. We have further improved the cycling stability of Li_2S electrodes by adding MWCNTs into the nanocomposite. With the highest specific energy (~610 W·h·kg^{-1}) demonstrated in this report, and with further improvement in capacity retention, this Li_2S–C nanocomposite electrode may offer a significant opportunity to go beyond traditional Li-ion cells toward the development of rechargeable batteries with much higher specific energy.

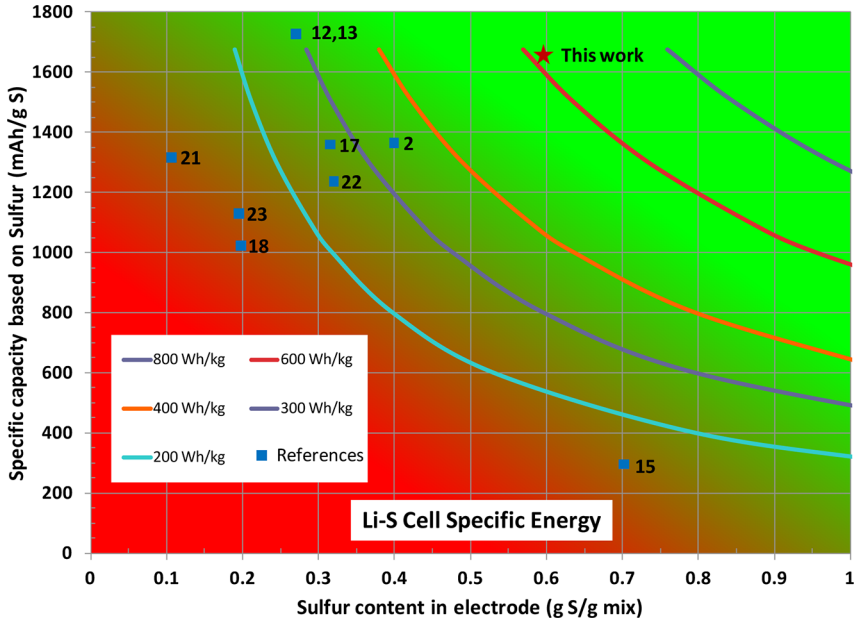

Figure 6. Estimated cell specific energy plot (including all components except the cell housing) as a function of the specific capacity based on S and the S content of the electrode. Previously reported data are marked by blue squares for comparison purposes, whereas the data of this work are indicated by the red star.

dx.doi.org/10.1021/nl303965a | *Nano Lett.* XXXX, XXX, XXX–XXX

■ ASSOCIATED CONTENT

Supporting Information

Additional figures and experimental details are included. This material is available free of charge via the Internet at http://pubs.acs.org.

■ AUTHOR INFORMATION

Corresponding Author

*E-mail: yzhang5@lbl.gov or ygzhang2012@sinano.ac.cn.

Present Addresses

[⊥]Permanent address for K. C.: State Key Laboratory of New Ceramics and Fine Processing, Department of Materials Science and Engineering, Tsinghua University, Beijing, 100084, China.

[#]Current address for Y. Z.: i-LAB, Suzhou Institute of Nano-Tech and Nano-Bionics, Chinese Academy of Sciences, Suzhou 215123, China. E-mail: ygzhang2012@sinano.ac.cn.

Author Contributions

[∥]These authors contributed equally to this work.

Notes

The authors declare no competing financial interest.

■ ACKNOWLEDGMENTS

This work was supported by the Office of Science, Office of Basic Energy Sciences, of the U.S. Department of Energy under contract No. DE-AC02-05CH11231.

■ REFERENCES

(1) Arico, A. S.; Bruce, P.; Scrosati, B.; Tarascon, J. M.; Van Schalkwijk, W. *Nat. Mater.* **2005**, *4* (5), 366−377.

(2) Yang, Y.; McDowell, M. T.; Jackson, A.; Cha, J. J.; Hong, S. S.; Cui, Y. *Nano Lett.* **2010**, *10* (4), 1486−1491.

(3) Tarascon, J. M.; Armand, M. *Nature* **2001**, *414* (6861), 359−367.

(4) Whittingham, M. S. *Chem. Rev.* **2004**, *104* (10), 4271−4301.

(5) Ji, X.; Lee, K. T.; Nazar, L. F. *Nat. Mater.* **2009**, *8* (6), 500−506.

(6) Etacheri, V.; Marom, R.; Elazari, R.; Salitra, G.; Aurbach, D. *Energy Environ. Sci.* **2011**, *4* (9), 3243−3262.

(7) Armand, M.; Tarascon, J. M. *Nature* **2008**, *451* (7179), 652−657.

(8) Marmorstein, D.; Yu, T. H.; Striebel, K. A.; McLarnon, F. R.; Hou, J.; Cairns, E. J. *J. Power Sources* **2000**, *89* (2), 219−226.

(9) Kobayashi, T.; Imade, Y.; Shishihara, D.; Homma, K.; Nagao, M.; Watanabe, R.; Yokoi, T.; Yamada, A.; Kanno, R.; Tatsumi, T. *J. Power Sources* **2008**, *182* (2), 621−625.

(10) Song, M.-K.; Park, S.; Alamgir, F. M.; Cho, J.; Liu, M. *Mater. Sci. Eng. Rep.* **2011**, *72* (11), 203−252.

(11) Cairns, E. J.; Albertus, P. Batteries for Electric and Hybrid-Electric Vehicles. In *Annual Review of Chemical and Biomolecular Engineering*, Vol. *1*; Prausnitz, J. M., Doherty, M. F., Segalman, M. A., Eds.; Annual Reviews: Palo Alto, CA, 2010; Vol. *1*, pp 299−320.

(12) Hassoun, J.; Scrosati, B. *Angew. Chem., Int. Ed.* **2010**, *49* (13), 2371−2374.

(13) Hassoun, J.; Sun, Y. K.; Scrosati, B. *J. Power Sources* **2011**, *196* (1), 343−348.

(14) Bruce, P. G.; Freunberger, S. A.; Hardwick, L. J.; Tarascon, J.-M. *Nat. Mater.* **2012**, *11* (1), 19−29.

(15) Takeuchi, T.; Sakaebe, H.; Kageyama, H.; Senoh, H.; Sakai, T.; Tatsumi, K. *J. Power Sources* **2010**, *195* (9), 2928−2934.

(16) Ji, X.; Nazar, L. F. *J. Mater. Chem.* **2010**, *20* (44), 9821−9826.

(17) Yang, Y.; Zheng, G.; Misra, S.; Nelson, J.; Toney, M. F.; Cui, Y. *J. Am. Chem. Soc.* **2012**, *134* (37), 15387−15394.

(18) Hayashi, A.; Ohtsubo, R.; Ohtomo, T.; Mizuno, F.; Tatsumisago, M. *J. Power Sources* **2008**, *183* (1), 422−426.

(19) Hayashi, A.; Ohtsubo, R.; Tatsumisago, M. *Solid State Ionics* **2008**, *179* (27−32), 1702−1705.

(20) Obrovac, M. N.; Dahn, J. R. *Electrochem. Solid-State Lett.* **2002**, *5* (4), A70−A73.

(21) Takeuchi, T.; Kageyama, H.; Nakanishi, K.; Tabuchi, M.; Sakaebe, H.; Ohta, T.; Senoh, H.; Sakai, T.; Tatsumi, K. *J. Electrochem. Soc.* **2010**, *157* (11), A1196−A1201.

(22) Fang, X. P.; Guo, X. W.; Mao, Y.; Hua, C. X.; Shen, L. Y.; Hu, Y. S.; Wang, Z. X.; Wu, F.; Chen, L. Q. *Chem.-Asian J.* **2012**, *7* (5), 1013−1017.

(23) Nagao, M.; Hayashi, A.; Tatsumisago, M. *J. Mater. Chem.* **2012**, *22* (19), 10015−10020.

(24) Rao, B. M. L.; Shropshire, J. A. *J. Electrochem. Soc.* **1981**, *128* (5), 942−945.

(25) Ji, L. W.; Rao, M. M.; Aloni, S.; Wang, L.; Cairns, E. J.; Zhang, Y. G. *Energy Environ. Sci.* **2011**, *4* (12), 5053−5059.

(26) Rao, M.; Song, X.; Cairns, E. J. *J. Power Sources* **2012**, *205*, 474−478.

(27) Han, S. C.; Song, M. S.; Lee, H.; Kim, H. S.; Ahn, H. J.; Lee, J. Y. *J. Electrochem. Soc.* **2003**, *150* (7), A889−A893.